

Planar Rayleigh scattering results in helium-air mixing experiments in a Mach-6 wind tunnel

B. Shirinzadeh, M. E. Hillard, R. Jeffrey Balla, I. A. Waitz, J. B. Anders, and R. J. Exton

Planar Rayleigh scattering measurements with an argon-fluoride excimer laser are performed to investigate helium mixing into air at supersonic speeds. The capability of the Rayleigh scattering technique for flow visualization of a turbulent environment is demonstrated in a large-scale, Mach-6 facility. The detection limit obtained with the present setup indicates that planar, quantitative measurements of density can be made over a large cross-sectional area ($5\text{ cm} \times 10\text{ cm}$) of the flow field in the absence of clusters.

Introduction

Instantaneous, nonintrusive measurements of flow fields play an important role in fluid mechanics. Various laser-based techniques that utilize pulsed lasers may be employed to acquire flow visualization data. Some of these techniques require seeding the flow with a species that exhibits large scattering cross sections.^{1,2} In supersonic and hypersonic facilities, where seeding presents environmental or technical problems, the Rayleigh scattering technique may be utilized for flow visualization.^{3,4} Investigations of the Rayleigh scattering technique in supersonic flow fields indicate that the scattering could be caused predominantly by clusters that are formed as a result of cooling that takes place during the expansion process.^{5,6} An investigation of the pressure and temperature dependence of the Rayleigh signal in such an expansion indicates that the signal is strongly dependent on the local values of these quantities in the flow.^{7,8} Here we present the results of our planar Rayleigh scattering measurements that were performed on a three-injector model designed by the California Institute of Technology (Caltech). The motivation was to investigate the unsteady component of hydrogen mixing into air at Mach 6 in a scramjet engine. Since the injection of hydrogen was not possible in this facility, it was replaced by helium injection because the flow properties exhibited by both species are similar. The Rayleigh scat-

tering results are presented along with a comparison of the Rayleigh data with mean flow parameters obtained from probe measurements performed by Caltech. This comparison elucidates the range of usefulness of the Rayleigh technique for flow visualization of a turbulent environment and its limitation in the presence of clusters. We also discuss the present detection limit and demonstrate that planar, quantitative measurements of the density in such flow fields can be performed in the absence of clusters.

Experimental

The experiments were performed in the Mach-6, high Reynolds number facility at NASA Langley Research Center. The facility test section was modified to admit a UV excimer laser and to permit the visualization experiments. Helium was injected into the free stream from three nozzles at various stagnation conditions (varied stagnation pressure, temperature, and boundary layer) to simulate the mixing of hydrogen into air at Mach 6. Because of a large difference in the Rayleigh cross section (a factor of ~ 100 at 193 nm) between helium and air in the molecular regime, one would expect to see no Rayleigh signal at a point where the helium is present at large concentrations in the flow.

Figure 1 shows a diagram of the injector model used for these experiments. In the design of the injector, the concept of shock-generated streamwise vorticity has been utilized to enhance mixing of fuel into air in scramjet combustors.^{9–12} The geometry permits formation of strong pressure gradients in proximity to fuel-air density gradients, providing vorticity generation by means of a baroclinic torque. The shock-generated vorticity is a loss-effective

B. Shirinzadeh, M. E. Hillard, R. J. Balla, J. B. Anders, and R. J. Exton are with the NASA Langley Research Center, Hampton, Virginia 23665; I. A. Waitz is with the California Institute of Technology, Pasadena, California 91125.

Received 27 August 1991.

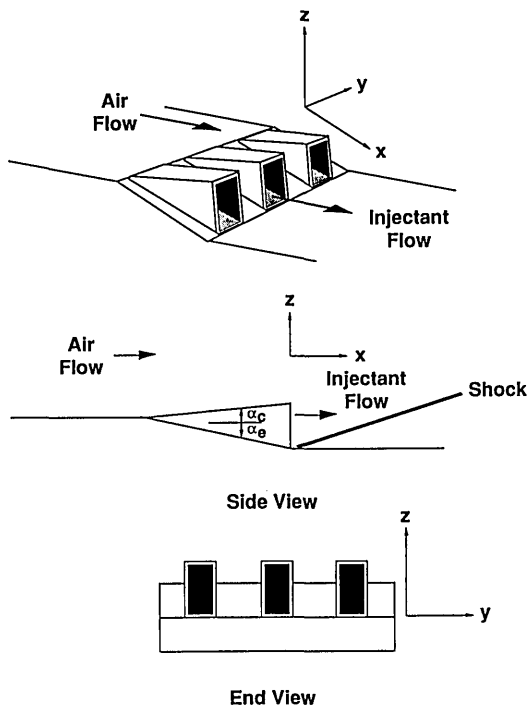


Fig. 1. Illustration of the model geometry.

method of enhancing mixing and alleviating adverse heating at the combustor wall. The fuel is injected parallel to the intended thrust vector, which provides full utilization of the momentum of the injectant. The planar images presented in this study were obtained at 10 injector heights downstream of the injection plane.

Figure 2 shows a schematic of the Rayleigh experimental setup. In these experiments, the output of a dual-cavity (oscillator and amplifier) argon-fluoride pulsed laser with a pulse duration of 15 ns, and a repetition rate of 10 pulses per second was used as the light source. The broadband output near 193 nm was formed into a sheet with a thickness of ~1 mm

and a height ranging from 2.8 to 6 cm by a series of cylindrical lenses (CL1 through CL4). The height of the sheet was varied, depending on the measurement station and the resolution required. The beam traversed the test section through two wedged windows and a series of apertures. The Rayleigh scattered light that was generated in this experiment was imaged onto a gated, single-intensified, CCD. An intensifier gate duration of 90 μ s was used to remove room light. The video signal from the camera was fed into a distribution amplifier. One output was digitized by a frame grabber and stored in a computer while the second output was stored by a video recorder. The video level was also monitored to ensure that the detection electronics were not in a saturation regime. In this way, a planar image of the Rayleigh scattered light was obtained.

To improve the detection limit of the Rayleigh scattering instrument, it was necessary to minimize the losses in laser energy, to reduce the background light from windows and walls, and to maximize the solid angle of collection. The first task was accomplished by purging the path of the beam between the laser and the test section window by using pure nitrogen. This reduced the absorption of the beam by molecular oxygen.^{13,14} Rectangular apertures were placed between the optics to reduce scattered light and to trap the back reflections. The output energy of the laser was ~130 mJ/pulse after the amplifier. Approximately one-half of this energy was lost by the end of the optical train, so that the usable energy was typically ~60 mJ/pulse. To minimize the effect of the laser light scattered by the windows and walls, rectangular (50.8 mm \times 127 mm) wedged windows were used. Apertures were designed to capture the 4% reflections caused by the windows and to limit the height of the beam inside the test section. All the surfaces inside the tunnel, including the model, were constructed from stainless steel that had a low reflectivity of ~5% at 193 nm (the reflectivity increases with wavelength). This overall design provided the capability of making measurements to within 3 mm above the model surface with negligible background signal. Finally, an imaging system, which consisted of two 50.8-mm-diameter lenses with focal lengths of 30.5 and 15.2 cm, was used to optimize the solid angle of collection. The imaging lenses were placed at a distance of ~76 cm from the plane of observation. The magnification of the lens system at 193 nm was determined experimentally to be ~6. The CCD camera consisted of a two-dimensional pixel array (384 \times 488) in which the dimension of each pixel was 30 μ m \times 18 μ m. An effective resolution obtained with this lens and camera system was ~1 mm in the plane of observation. When the maximum gain was used on the intensifier, we observed that a 2.5-Torr pressure change at room temperature would result in a one-count change in the digitized camera signal. At this maximum gain, a single-shot detection limit of 2×10^{17} air molecules/cm³ was estimated. Since, under a typical operating condition (i.e., $P_t = 1000$

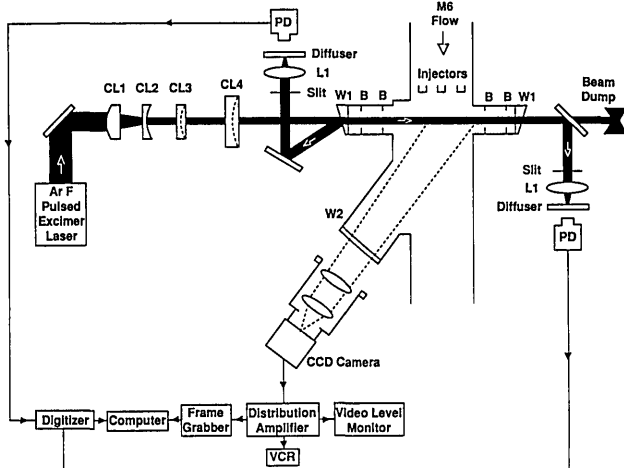


Fig. 2. Schematic diagram of the experimental setup. CL's, cylindrical lenses; W's, windows; B's, baffles; L's, spherical lenses; PD's, photodiodes.

psi, $T_t = 475^\circ\text{F}$), the free-stream density in this facility is $\sim 5 \times 10^{18}$ molecules/cm³, this detection limit is sufficient to perform planar Rayleigh scattering measurements of the flow field in the absence of any clusters in the free stream of this facility.

To minimize uncertainties associated with the photon flux, the volume of interaction, the solid angle of collection, the transmission of optics, the quantum efficiency, and the gain difference between different pixels on the CCD, it was necessary to calibrate the laser-camera system. This calibration was performed, as before,^{7,8} by pumping the test section down to a range of pressures of interest and by obtaining the Rayleigh scattering measurements at these known air pressures. For these experiments, 22 images were averaged for each pressure and normalized to the average energy. For each pixel, a linear plot of the Rayleigh signal as a function of the pressure was obtained. By using a linear least-squares-fitting routine, we determined the slope and the intercept with their associated uncertainties and stored them in a file. The flow-field data were converted to pressure data at room temperature by using this calibration file. This procedure removes the systematic nonuniformities in the laser-camera system.

During the time that the tunnel was operational, it was not possible to enter the facility. To verify the stability of the laser, the energy output was measured before and after the test section. To do this, a small portion of the beam was directed to a lens, which reduced the beam size. The beam was then diffused by a scatter plate and was detected by a fast photodiode. The signal output of the detector was processed by sample and hold detection, and was digitized and stored in the computer. This provided us with a measure of the average laser energy that was used for normalization of the signal. To minimize the shot-to-shot variations in the intensity a section of the frame with a constant pattern was chosen, and the entire image was then normalized to the averaged value of the signal in that section. This procedure minimizes the combined effect of the laser intensity and the flow-field fluctuations caused by variations in stagnation conditions.

Finally, to be able to compare the planar Rayleigh images with both the probe data and the computational fluid-dynamics (CFD) calculations, it was necessary to convert the position of each pixel to the actual position in a plane perpendicular to the flow in the tunnel. To do so, a square grid constructed from a plate of aluminum was placed perpendicularly to the flow direction such that the bottom of the grid was flush with the surface of the model and its center was coincident with the center of the model. In the beginning of each run, after all the adjustments on the laser beam and the camera system were made, the grid was placed at the position of the laser beam and was illuminated by some scattered laser light at 193 nm. An image of the grid was obtained and used to convert the pixel array to a spatial position in a plane

perpendicular to the flow. This procedure permitted a spatial comparison between the Rayleigh images and both the probe data and the CFD calculations.

Results and Discussion

Figure 3 shows a plot of two consecutive Rayleigh images obtained at 10 injector heights downstream from the injectors. These data were obtained for the condition of matched helium and air static pressures with a helium stagnation temperature of ~ 300 K. The Rayleigh signal has been converted to pressure at room temperature by using the calibration file. In addition, each image has been normalized to the average value obtained in the rectangular area shown in the figure. Because of the cluster formation in the tunnel, it was not possible to set the intensifier gain to the maximum value under these experimental conditions ($P_t = 600$ psi, $T_t = 475^\circ\text{F}$). The gain was set experimentally to avoid saturation and remained constant throughout the experiments. For this run condition, the intensifier gain was set to give a one-count change in the camera signal for every 8 Torr of pressure at room temperature. (The maximum number of counts available was 2⁸.) The deduced calibration intercept reflected the preset threshold of ~ 12 counts on the digitizer. The maximum statistical uncertainties for the deduced slope and intercept were $\sim 7\%$ and 20%, respectively. These uncertainties defined a detection threshold of ~ 16 Torr for our system in this case. For the data presented in Fig. 3, low signal levels that are below our detection threshold have been assumed to be equal to zero (black area in the picture) for the purpose of presentation. The symmetric structure outside the helium region and the reproducibility of

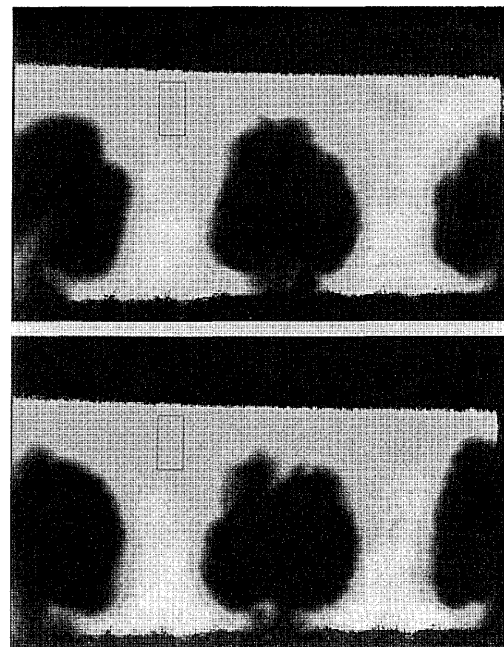


Fig. 3. Corrected Rayleigh images for two consecutive laser shots. See text for details.

this structure from shot to shot (Fig. 3) indicates that the calibration and the normalization procedures described above work well for this flow field. The large signal levels observed point to the presence of clusters, which complicates the interpretation of the Rayleigh data and requires instrumentation with a large dynamic range. In fact, when the tunnel was operated at a stagnation pressure of $P_t = 1000$ psi (same stagnation temperature), we observed a band of large signal levels around the helium region (not present in these data) that dominated the flow-field image. This indicates that, when using the Rayleigh scattering process for flow visualization in the presence of clusters, one must be extremely careful. To avoid this, we were forced to operate at a lower stagnation pressure of 600 psi. At this pressure, the bright band disappeared.

For comparison between the probe and the Rayleigh scattering measurements, probe data were obtained at a stagnation pressure of 700 psi. A detailed description of the probe measurement technique is outside the scope of this paper and can be found in Ref. 11. Here we only list the measurements and discuss the sources of uncertainty. Pitot pressure, cone static pressure, total temperature, and composition measurements were made over a two-dimensional grid of 140 discrete points. The composition data were obtained by using a sonic, aspirated, hot-film-based, gas sampling apparatus. The apparatus permitted measurements of the helium mole fraction with an uncertainty of no more than 3%. The raw data were mirrored about the axis of symmetry of the jet and were reduced to obtain base flow variables (e.g., density and static temperature). The reduc-

tion of the raw survey data was based on iterating the system of ordinary differential equations that describe conical flow and Pitot pressure relation in P_∞ and M_∞ for gas properties defined by the composition and total temperature measurements. An effective cone angle was adopted to correct the data for Reynolds number effects. The correction had no uniform validity throughout the flow field. Misalignment of the probes, significant flow angularity in some regions, and sensitivity of the reduction technique to uncertainty in the raw data further limited the extent to which the reduced data could be relied on to represent accurately characteristics of the flow field. The reduced data were used to provide only a rough quantitative measure of base flow variables.

A comparison between the averaged Rayleigh data [in units of pressure (Torr) at room temperature] and both the mass density (in units of kg/m^3) of air and the static temperature (in units of Kelvin) deduced from the probe measurements in the flow field are presented in Fig. 4. In this figure, the Rayleigh data [which are labeled as (a)] are rotated to represent viewing along a direction parallel to the flow, and y and z are the actual horizontal and vertical spatial coordinates, respectively, normalized to one injector height [the injector measured 1 in. (2.54 cm) in height and 0.5 in. (1.27 cm) in width]. These data were obtained for the same test condition described above and represent the average flow field (22 laser shots) for the central injector. Again, by using the calibration file, we have converted the Rayleigh signals to pressure (Torr) at room temperature. It is seen from Fig. 4 that the qualitative agreement between the Rayleigh results and the deduced mass density of

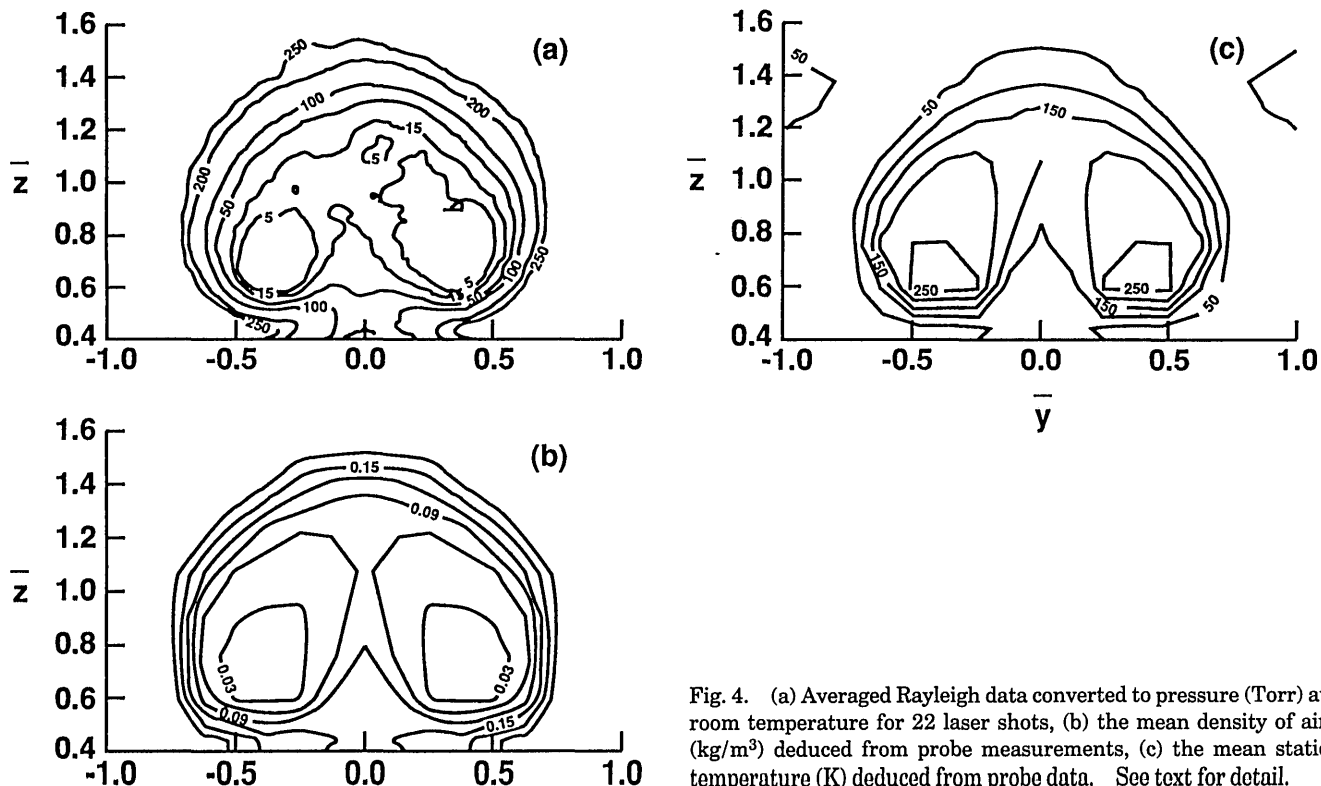
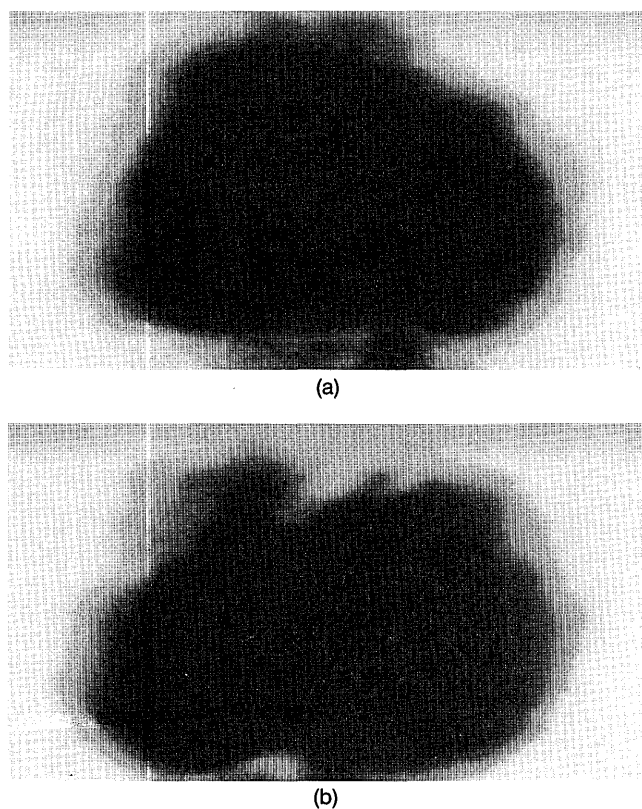


Fig. 4. (a) Averaged Rayleigh data converted to pressure (Torr) at room temperature for 22 laser shots, (b) the mean density of air (kg/m^3) deduced from probe measurements, (c) the mean static temperature (K) deduced from probe data. See text for detail.

air [Fig. 4(b)] from the probe measurements is remarkable. The shape of the density gradients in both data sets is the same. That is, in spatial regions in which the probe data undergo a rapid change in density, the Rayleigh data also does the same but with a different magnitude. The static mean temperatures [Fig. 4(c)] deduced from the probe measurements exhibit a large variation from 40 to 250 K in this flow field. As a result, the strong dependence of the cluster formation process on the local temperature and pressure^{7,8} in the flow field creates a large variation in the Rayleigh signal. Nevertheless it is seen that the variations in the Rayleigh signal correlate well with the mean-air-density gradients deduced from probe data. In the flow regions exhibiting high static temperatures, the Rayleigh signal may be generated by air molecules only. However, the turbulent nature of the flow (which is discussed below) prohibits us from making a quantitative comparison between the average mass density deduced from the probe measurements and the Rayleigh results in those flow-field regions.

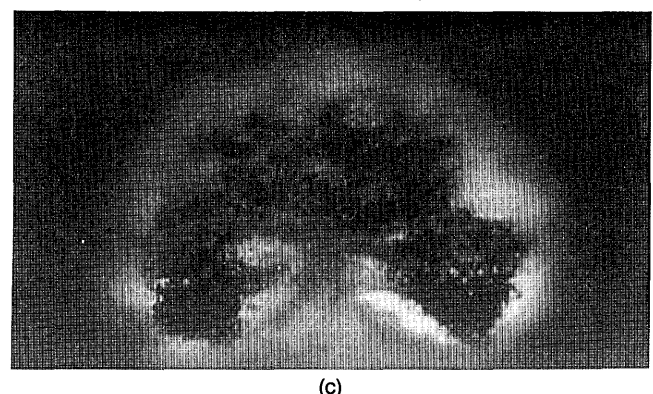
The greatest utility of the Rayleigh images in terms of defining injector performance was not representation of time-mean data, but rather a qualitative display of the fluctuating component of the flow field. Determining the scale and the importance of the unsteady component of the flow field is vital in properly interpreting the detailed mean flow data obtained from the probe measurements. Figure 5 shows the single-shot data obtained for this run condition for the central injector. In Fig. 5, two

consecutive laser shots, labeled (a) and (b), are shown in the same coordinate system as in Fig. 4. These data have been processed in the same manner discussed above. Since the laser pulse duration is 15 ns, the flow is considered frozen for this single-shot data. From these pictures, the turbulent nature of the flow is evident. To estimate the extent of this turbulence, we calculated the fluctuating component for 22 images labeled as (c) in Fig. 5. This computation was performed by considering the nonzero values of the pressure deduced for single-shot data and calculating the mean and the standard deviation of the mean value for these nonzero values. The relative standard deviation of this nonzero component represents the fluctuating component. This procedure enhances the fluctuating component at the boundary between helium and air in the flow field but decreases the effect of low signal levels, in which the frequency of occurrence of a nonzero component is small. In other words, the dark area inside the helium region in Fig. 5(c) does not indicate that the flow is steady there, but it reflects near-zero signal levels. On the other hand, the dark region outside the helium core reflects steadiness of the flow field in that region. In Fig. 5(c) it is also seen that the region in which the fluctuating component is the largest (20%) appears to correlate with the static mean-temperature plot shown in Fig. 4(c). That is, regions with large temperature gradients also show higher fluctuating components. Since each image has been normalized to the averaged value of the signal in a section of the same frame, the fluctuations



(a)

(b)



(c)

Fig. 5. (a) Corrected single-shot image of the Rayleigh signal for the central injector, (b) the same as (a) but for another laser shot in the same sequence, (c) the fluctuating component of the Rayleigh signal for 22 laser shots in the same sequence. See text for detail.

observed cannot be due to the change in the laser energy or the stagnation conditions (note that outside the helium region the fluctuating component is nearly zero). In addition, the overall agreement between the averaged Rayleigh results and the deduced mean density indicates that, under these experimental conditions, the clusters enhance the effect of variations in the thermodynamic parameters.

Conclusions

In this paper, we have demonstrated the capability of the Rayleigh scattering technique for flow visualization of a turbulent environment in a large-scale, Mach-6 facility. We have shown that useful fluid mechanics information, such as the turbulent nature of the flow, can be derived from the single-shot data. In addition, the qualitative agreement between the averaged Rayleigh result and the reduced mean-mass density obtained from the probe measurements further substantiate that careful application of the technique, even in the presence of clusters, can give useful results. We have also demonstrated that planar, quantitative measurements can be made in the absence of clusters.

The authors thank Ray Gregory for the design and implementation of the control circuit for the data acquisition system, Bruce Barnes and Bill Chambers for the expert mechanical design and assembly of the structure supporting the laser and optics, Kelly Debare for her image processing skills, and the facility operators for their skill in providing conditions for *in situ* calibrations and for obtaining stagnation conditions beyond typical facility operation.

References

1. R. J. Hartfield, Jr., J. D. Abbott III, and J. C. McDaniel, "Injectant mole-fraction imaging in compressible mixing flows using planar laser-induced iodine fluorescence," Opt. Lett. **14**, 850-852 (1989).
2. N. T. Clemens, P. H. Paul, M. G. Mungal, and R. K. Hanson, "Scalar mixing in the supersonic shear layer," AIAA paper 91-1720 (American Institute of Aeronautics and Astronautics, New York, 1991).
3. M. Smith, A. Smits, and R. Miles, "Compressible boundary-layer density cross sections by UV Rayleigh scattering," Opt. Lett. **14**, 916-918 (1989).
4. R. W. Dibble, R. S. Barlow, M. G. Mungal, K. Lyons, B. Yip, and M. B. Long, "Visualization of supersonic flows with planar laser Rayleigh scattering," Sandia Rep. SAND89-8401 (Sandia National Laboratories, Livermore, Calif., 1989).
5. G. D. Stein, "Angular and wavelength dependence of the light scattered from a cloud of particles formed by homogeneous nucleation," J. Chem. Phys. **51**, 938-942 (1969).
6. P. P. Wegener, "Nucleation of nitrogen: experiment and theory," J. Phys. Chem. **91**, 2479-2481 (1987).
7. B. Shirinzadeh, M. E. Hillard, and R. J. Exton, "Condensation effects on Rayleigh scattering measurements in a supersonic wind tunnel," AIAA J. **29**, 242-246 (1991).
8. B. Shirinzadeh, M. E. Hillard, A. B. Blair, and R. J. Exton, "Study of cluster formation and its effects on Rayleigh and Raman scattering measurements in a Mach 6 wind tunnel," AIAA paper 91-1496 (American Institute of Aeronautics and Astronautics, New York, 1991).
9. F. E. Marble, G. J. Hendricks, and E. E. Zukoski, "Progress toward shock enhancement of supersonic combustion processes," AIAA paper 87-1880 (American Institute of Aeronautics and Astronautics, New York, 1987).
10. F. E. Marble, E. E. Zukoski, J. W. Jacobs, G. J. Hendricks, and I. A. Waitz, "Shock enhancement and control of hypersonic mixing and combustion," AIAA paper 90-1981 (American Institute of Aeronautics and Astronautics, New York, 1990).
11. I. A. Waitz, "An investigation of contoured wall injectors for hypervelocity mixing augmentation," Ph.D. dissertation (California Institute of Technology, Pasadena, Calif., 1991).
12. I. A. Waitz, F. E. Marble, and E. E. Zukoski, "An investigation of contoured wall injectors for hypervelocity mixing augmentation," AIAA paper 91-2265 (American Institute of Aeronautics and Astronautics, New York, 1991).
13. M. P. Lee and R. K. Hanson, "Calculations of O₂ absorption and fluorescence at elevated temperatures for a broadband argon-fluoride laser source at 193 nm," J. Quant. Spectrosc. Radiat. Transfer **36**, 425-440 (1986).
14. L. M. Hitchcock, G. Kim, G. P. Reck, and E. W. Rothe, "Absorption of laser light in air in the 193 nm range: analysis of laser locking," J. Quant. Spectrosc. Radiat. Transfer **44**, 373-378 (1990).